Journal of Engineering and Technological Sciences

Research Paper

Sensitive Detection of Rhodamine B Using Surface Enhanced Raman Spectroscopy with a $BiFeO_3$ based Substrate

Diva Cassia Mayora[1], Djoko Triyono[1,*], Muhandis Shiddiq[2], Rifqi Almusawi Rafsanjani[1], & Akhmad Futukhillah Fataba Alaih[1]

[1]Departement of Physics, Faculty of Mathematics and Natural Sciences, University of Indonesia, Lingkar Street, Depok, West Java, 16424, Indonesia
[2]Research Center for Photonics, National Research and Innovation Agency (BRIN), Raya Puspiptek Street, Puspiptek, Tangerang Selatan, Banten, 15314, Indonesia

*Corresponding author: djoko.triyono@sci.ui.ac.id

Abstract

Surface-Enhanced Raman Spectroscopy (SERS) is a highly effective technique for detecting trace amounts of molecular species. However, the widespread use of conventional noble metal substrates is limited by high fabrication costs and scalability issues. Perovskite materials have recently emerged as promising alternatives, though many are lead-based and pose environmental risks. In this study, we present a lead-free bismuth ferrite ($BiFeO_3$) perovskite synthesized via the sol–gel method as a novel SERS substrate for the detection of Rhodamine B, a toxic dye commonly used illicitly in food products. Comprehensive characterization using X-ray Diffraction (XRD), X-ray Fluorescence (XRF), and UV-Visible Diffuse Reflectance Spectroscopy confirmed the successful formation of a single-phase rhombohedral structure with a direct bandgap of 2.1 eV, indicating strong visible-light absorption. The $BiFeO_3$ substrate demonstrated effective SERS performance, facilitating a detection of Rhodamine B at concentrations as low as 10 ppm. These results highlight the potential of lead-free $BiFeO_3$ perovskites as practical and environmentally friendly alternatives to noble metals for SERS-based detection of hazardous dyes and other environmental contaminants.

Keywords: *bismuth ferrite; perovskite; rhodamine B; sers substrate; synthetic dyes.*

Introduction

Raman spectroscopy is a method that uses the vibrational spectrum of chemical bonds in a molecule and has consideration to changes that happen in its surroundings (Hidayah et al., 2022). Then, in the characterization of chemical and physical properties, Raman spectroscopy becomes a critical instrument because its spectral pattern holds uncommon information about a compound that grants for molecular identification. The severity of the Raman signal is known as a weak signal but can be notably increased if the molecule is adsorbed on a coarse metal surface or metal nanoparticles. Surface-Enhanced Raman Spectroscopy (SERS) is the name of this method (Hidayah et al., 2022). The SERS technique is a potent analytical approach that notably amplifies Raman signals, authorizing the detection of molecules at very low concentrations, even to the single-molecule level (Q. Wang et al., 2025). This method has been rapidly used in many areas, such as chemical sensing, environmental monitoring, biomedical diagnosis, and food safety monitoring. The observed enhancement stems from electromagnetic (EM) and chemical or charge-transfer mechanisms (CT) (Cui et al., 2025). The enhancement of the EM in SERS mainly arises from the plasmonic properties of metallic nanoparticles, which generate localized surface plasmons upon light excitation. In contrast, the CT, which is more significant in semiconductors, involves photoinduced charge exchange between the substrate and the adsorbed analyte molecules (Anucha et al., 2025).

In the past, noble metals were mainly used because of their strong electromagnetic enhancement. However, with the development of material science, researchers have started exploring other materials for SERS substrates, including semiconductors such as TiO_2, ZnO, and silicon-based compounds, as well as two-dimensional materials like MoS_2 and graphene (Yin et al., 2022). Among these, perovskite materials stand out as especially promising alternatives. Perovskite ceramics are simple ionic compounds with the general chemical formula ABO_3, where ion A is generally large, while ion B is medium in size (Triyono et al., 2019). This material has many unique characteristics that make them ideal for SERS

ISSN: 2337-5779
J. Eng. Technol. Sci. Vol. 57, No. 6, 2025, 875-884
DOI: 10.5614/j.eng.technol.sci.2025.57.6.10

applications, including high light absorption, a direct band gap, large charge carrier mobility, and tunable electronic properties—all of which contribute to efficient CT (Pan et al., 2022). Unlike noble metals, perovskites can be synthesized by more cost-effective methods, making them an attractive choice for large-scale sensing applications.

Over the last few years, interest in the use of perovskite-based materials as potential substrates for SERS has increased significantly (Pan et al., 2022). These materials generally amplify Raman signals through the CT mechanism, which can display complementary or even synergistic effects when merged with plasmonic phenomena, and it's opposed to metals (J. Tian, 2023). Normally, research on perovskite-based SERS has concentrated on materials carrying lead (Pb) (Pan et al., 2022; 2023), which raise concerns about toxicity and often requires complex synthesis method such as vacuum deposition or stepwise composite fabrication. These minuses make it hard to test the potential for scalability and widespread practical application. To get over these minuses, nowadays research has started focusing on lead-free and easier-to-synthesize alternative materials, for an example bismuth ferrite ($BiFeO_3$) (Jain et al., 2025)

$BiFeO_3$ is known as multiferroic perovskite semiconductor, that displays both ferroelectric and antiferromagnetic properties in the room temperature (Sarkar et al., 2024). Due to its relatively tiny band gap (~2.1–2.7 eV), this material has recently got a lot of attention as an encouraging possibility for a bunch of research applications (Zhou et al., 2023). This material also has the ability to absorb visible light perfectly, so it is a potential nominee for a lot of photoactive applications (Sahoo et al., 2024). $BiFeO_3$ is known for its safety and stability, as well as its ability to be immune to light-induced damage. These outcomes make it a valid material for sensing applications that work in a wide scale of environmental conditions (Liu et al., 2020). From the structure based, the valence band of bismuth-based oxides is primarily formed by the hybridization with both Bi-6s and O-2p orbitals, which produce strong interactions. This interaction will improve the oxidizability of the material and assist efficient charge transfer processes, which take a main role in Raman enhancement based on the CT mechanism (Kokhilavani et al., 2022). Due to its distinctive propensity, $BiFeO_3$ outshines as a good semiconductor-based SERS substrate, proficient of bringing out Raman signal amplification without the involvement of noble metals. Its response to visible light, stability of the structure, and eco-friendly chemical character make it a perfect choice for sensitive and sustainable molecular observation (Zhou et al., 2023).

We centre on the synthesis, characterization, and application of $BiFeO_3$ perovskite as a novel SERS active substrate in this study. Especially, we explore its performance in finding trace levels of Rhodamine B—a synthetic xanthene dye with the molecular formula $C_{28}H_{31}ClN_2O_3$. Rhodamine B is usually used in some industries such as textiles and cosmetics due to its intense fluorescence and inexpensiveness (Bashir et al., 2025). Though, it has been grouped as a possibly carcinogenic compound, with described neurotoxic, developmental, and reproductive toxicities, posing significant health risks to both humans and animals (Nithish et al., 2025). Even with regulatory restrictions, Rhodamine B continues to be illegally added to food products in some regions, making the detection of even trace levels of Rhodamine B critically important for public health and safety.

To the best of our knowledge, there have been no prior reports on the use of $BiFeO_3$ perovskite as a SERS substrate for the detection of Rhodamine B. Therefore, this work aims to explore the untapped potential of $BiFeO_3$ in SERS applications, demonstrating not only its material properties but also its effectiveness in enhancing the Raman signals of Rhodamine B at low concentrations. This research may open new avenues for the development of lead-free, cost-effective, and eco-friendly SERS platforms for real-world detection of hazardous dyes and other environmental contaminants.

Materials and Methods

Materials

$Fe(NO_3)_3{\cdot}9H_2O$ (Sigma-Aldrich), $Bi(NO_3)_3{\cdot}H_2O$ (Sigma-Aldrich), Citric Acid (Merck), Polyethylene Glycol (Merck), and aquabidest were used for the synthesis of $BiFeO_3$. Additionally, acetone (Merck), isopropanol (Merck), and silicon wafer (Zhongding) were used for substrate fabrication. Powdered Rhodamine B was used to make the Rhodamine B solution for the SERS measurement. The $BiFeO_3$ crystal phase was examined by X-ray diffraction (XRD) using a PANalytical X'Pert Pro diffractometer. Measurements were carried out with Cu Kα radiation (λ = 1.5418 Å) across a 2θ range from 10° to 80°. Optical characteristics were analyzed with an Agilent Cary 100 UV–Vis spectrophotometer, covering the wavelength range of 200–800 nm. The direct band gap was estimated by applying the modified Kubelka-Munk function to construct a Tauc plot, illustrating the relationship between $[F(R)hv]^2$ and (hv). The chemical composition and the concentration of elements in the sample was measured using the X-Ray Fluorescence Spectroscopy (XRF) instrument Ɛ1: Malvern

DOI: 10.5614/j.eng.technol.sci.2025.57.6.10

Panalytical with an Ag radiation source and a voltage of 50 kV. The SERS performance was measured with Raman HR 550 (Horiba Jobin Yvon) with 785 nm laser, 250 mW power, and 1800 grooves/mm grating.

Synthesis of $BiFeO_3$

$BiFeO_3$ powders were synthesized via a modified sol–gel method based on procedures reported by Mhamad et al. (2022). Bismuth (III) nitrate pentahydrate [$Bi(NO_3)_3{\cdot}5H_2O$] and ferric nitrate nonahydrate [$Fe(NO_3)_3{\cdot}9H_2O$] were used as precursors. A stoichiometric number of precursors (1:1 molar ratio of Fe^{3+} to Bi^{3+}) were separately dissolved in 200 mL distilled water under continuous magnetic stirring. The solution was then added with citric acid and polyethylene glycol with (1:1) molar ratio with metal nitrate which act as chelating agents, and the solution was kept under constant stirring at 120°C for 24 hours. Next, the gel was acquired and dried at 150°C for 24 hours. By that, to induce crystallization of the perovskite phase and acquire $BiFeO_3$ powder with high phase purity and crystallinity, the sample was calcinated at 650°C for 6 hours (Triyono et al., 2019). The $BiFeO_3$ powder was then obtained.

Substrate Fabrication

Coating solution of perovskite was made with 120 mg of the synthesized $BiFeO_3$ powder combined with 2.1 mL of ethanol and 0.9 mL of distilled water. The mixture was then ultrasonicated with homogenizer for three hours to disperse the $BiFeO_3$ particles. This process made a smooth and homogeneous perovskite ink, which was suitable for thin film fabrication. Next, the $BiFeO_3$ substrate was prepared using the drop-casting method. Silicon wafer was first cut into 0.5 cm × 0.5 cm squares and meticulously cleaned through sequential rinses in acetone, isopropanol, and aquabidest, followed by air drying. After cleaning, 0.1 mL of the $BiFeO_3$ solution was dropped onto the surface of the silicon wafer and allowed to dry under ambient room temperature. As the solvent evaporated, a thin and uniform $BiFeO_3$ film was formed on the substrate surface, serving as the active layer for SERS measurements.

SERS Measurement

To evaluate the SERS activity of the fabricated $BiFeO_3$ substrate, 5 µL of a 10 ppm Rhodamine B solution was dropped directly onto the coated surface. The sample was allowed to dry naturally, ensuring that the analyte was adsorbed onto the $BiFeO_3$ surface. The Raman signal of Rhodamine B was then measured using the previously mentioned Raman spectrometer setup. The characteristic peaks of Rhodamine were monitored and compared to control measurements (without $BiFeO_3$ or with bare silicon substrate) to assess the enhancement effect provided by the $BiFeO_3$ film.

Results

Characterization of X-Ray Diffraction

X-Ray Diffraction (XRD) was performed using a Malvern Panalytical diffractometer with Cu Kα radiation (λ = 1.5406 Å), scanned in the 2θ range of 10°–80°. Figure 1 displays the XRD pattern of the synthesized $BiFeO_3$ powder. The relatively small difference between the observed and calculated patterns is shown by the narrow blue difference line in Figure 1, which further supports the phase purity and structural accuracy of the synthesized $BiFeO_3$ material.

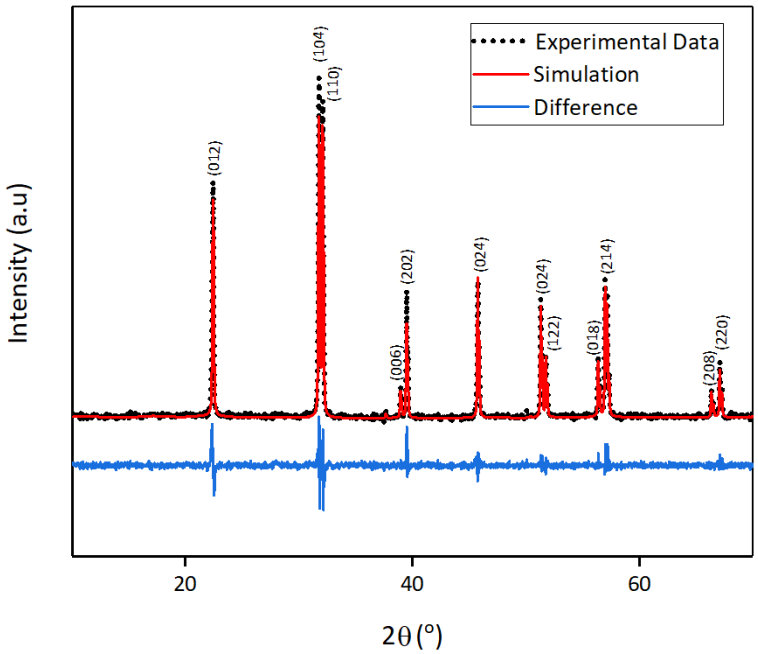

Figure 1 The XRD Spectra of $BiFeO_3$.

The corresponding lattice parameters and structural details are summarized in Table 1. The $BiFeO_3$ exhibits lattice constants a = b = 5.5761 Å and c = 13.8627 Å. The crystallite size was estimated to be 51.7 nm. The tolerance factor was calculated to be 0.91.

Table 1 Structure parameters of $BiFeO_3$.

Parameter	Value
Crystal Structure	Rhombohedral
Space Group	*R* 3 c
Lattice Parameter	
a (Å)	5.5761
b (Å)	5.5761
c (Å)	13.8627
Crystallite size (nm)	51.7
Tolerance factor (%)	0.91
R-Factor (%)	
Re	4.36870
Rp	5.07855
Rwp	6.93146

Characterization of X-Ray Fluorescence

X-Ray Fluoresence (XRF) was performed using Malvern Panalytical Ɛ1 instrument with an Ag radiation source of 50 kV. Table 2 presents the XRF results of $BiFeO_3$. The elemental composition obtained from XRF measurements shows good agreement with the theoretical stoichiometric values of $BiFeO_3$, with only minor deviations.

Table 2 The XRF Calculation of $BiFeO_3$.

%Weight from XRF Measurement		%Weight from Stoichiometric Calculation	
Bi	**Fe**	**Bi**	**Fe**
81.4	18.6	78.8	21.2

Characterization of UV-Vis Spectroscopy

UV-Vis Spectroscopy was performed using 100 UV-Vis Agilent Cary with wavelength of 200-800 nm. Figure 2(a) presents the diffuse reflectance spectrum (DRS) of the synthesized $BiFeO_3$ powder as a function of incident light wavelength,

DOI: 10.5614/j.eng.technol.sci.2025.57.6.10

measured in the UV-Visible range. The spectrum reveals a notable decrease in reflectance between 525–580 nm. Figure 2(b) shows the Tauc plot derived from the Kubelka–Munk function, which is used to determine the optical bandgap energy of powdered semiconductor materials. It shows the bandgap value of (2.1 eV).

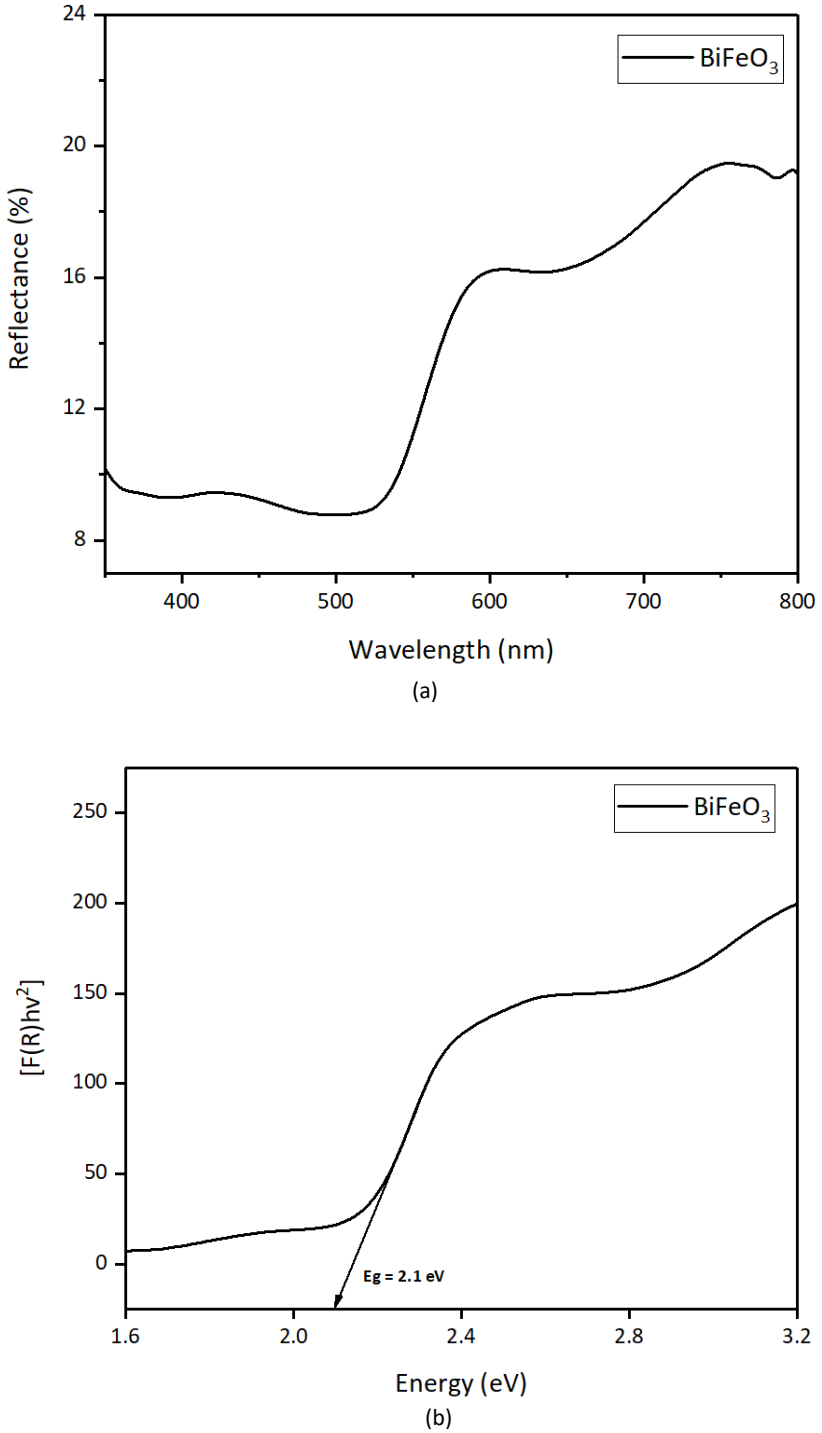

Figure 2 (a) UV-Vis Reflectance Spectrum of $BiFeO_3$, (b) The Bandgap of $BiFeO_3$ using Kubelka Monk method.

SERS Measurement

The SERS performance was evaluated using Raman HR 550 (Horiba Jobin Yvon) with a 785 nm laser, 250 mW power, and 1800 grooves/mm grating. Figure 3 displays the SERS spectra of: Rhodamine B on bare SiO_2 wafer (a), $BiFeO_3$ on bare SiO_2 wafer (b), and Rhodamine B deposited on a $BiFeO_3$ substrate on SiO_2 wafer (c).

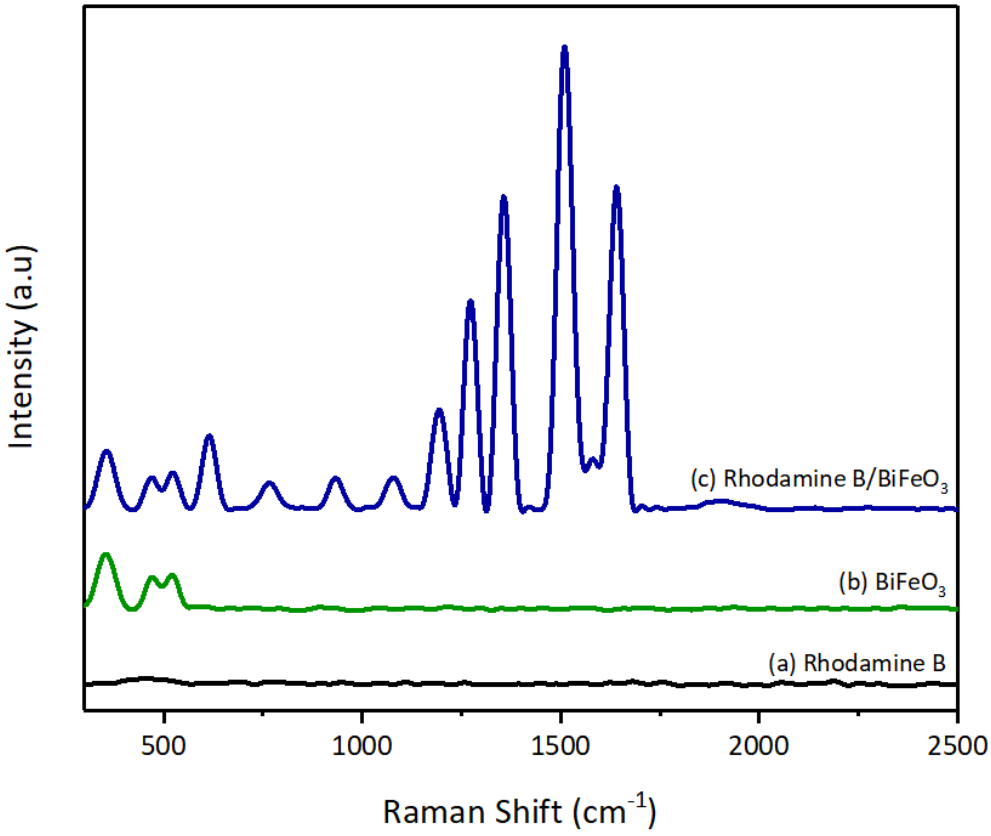

Figure 3 The Observed Raman Shift of **(A)** Rhodamine B on SiO_2 wafer, **(B)** $BiFeO_3$ on SiO_2 wafer, **(C)** Rhodamine B with $BiFeO_3$ substrate on SiO_2 wafer.

Table 3 shows the reported peaks that are correspond with the previous research (Y. Yang, 2009).

Table 3 SERS Peak Assignments of $BiFeO_3$ and Rhodamine B.

SERS peak (cm^{-1})	Assignment	References
	$BiFeO_3$	
370	E modes	(Fajriyani & Triyono, 2020)
470	E modes	(Fajriyani & Triyono, 2020)
520	A-1 modes	(Fajriyani & Triyono, 2020)
	Rhodamine B	
616	C_x-C_x-C_x bend	(Mao et al., 2023)
765	C_x-H out-of-plane bend	(Mao et al., 2023)
933	C_x-C_x-C_x bend	(Mao et al., 2023)
1079	C-H stretching	(Mao et al., 2023)
1193	C-C bridge band stretching and aromatic	(Mao et al., 2023)
1273	C-H bending	(Mao et al., 2023)
1357	Aromatic C-C bending	(Mao et al., 2023)
1510	C_x-C_x stretching	(Mao et al., 2023)
1640	C_x-C_x stretching	(Mao et al., 2023)

x = xanthene ring

Discussion

Based on the characterization of X-Ray Diffraction (XRD) of $BiFeO_3$, the observed diffraction peaks exhibit excellent agreement with the standard reference pattern (JCPDS 98-018-0506) for rhombohedral $BiFeO_3$, confirming the successful formation of the targeted crystal phase. The diffraction peaks are sharp and well-defined, indicating the high

DOI: 10.5614/j.eng.technol.sci.2025.57.6.10

crystallinity of the sample (Cebela et al., 2017). The lack of secondary or unidentified peaks indicates that the sample contains no impurity phases such as Bi_2O_3, Fe_2O_3, or $BiFe_2O_4$, which often appear when $BiFeO_3$ synthesis is not well controlled (Cebela et al., 2017). The crystallite size, estimated from the (110) peak using the Scherrer equation, was approximately 51.7 nm—closely matching with the values reported in earlier sol–gel-based $BiFeO_3$ studies (Mhamad et al., 2022), indicating that the particles fall within the nanometer range, which can enhance surface-dependent properties such as photocatalytic performance or SERS activity by providing a larger surface area and more active sites. The $BiFeO_3$ sample shows lattice constants of a = b = 5.5761 Å and c = 13.8627 Å, which align well with previously reported values for rhombohedral $BiFeO_3$ in the literature (Triyono et al., 2019). The calculated tolerance factor of 0.91 suggests that the material maintains structural stability within the perovskite framework, as values between 0.8 and 1.0 generally correspond to stable perovskite phases (Culbertson et al., 2020). Additionally, the R-factor values including Re (4.37%), Rp (5.08%), and Rwp (6.93%) are all within acceptable ranges, further confirming the reliability of the Rietveld refinement and the goodness of fit between the experimental and simulated patterns. Taken together, the XRD analysis demonstrates that the synthesized $BiFeO_3$ powder is single-phase, highly crystalline, and structurally consistent with the standard $BiFeO_3$ perovskite model. These characteristics are expected to enhance charge-transfer processes and surface interactions, contributing to stable and strong SERS signals. Similar structure–performance correlations have been observed in other semiconductor nanoparticles, where well-defined crystal structures and controlled sizes markedly improved detection sensitivity (Zhuang et al., 2024)

The X-Ray Fluorescence (XRF) Characterization shows the elemental composition obtained from XRF measurements which shows good agreement with the theoretical stoichiometric values of $BiFeO_3$, with only minor deviations. These slight differences may be attributed to experimental uncertainties or instrumental limitations inherent in XRF analysis. However, it is important to note that XRF is generally insensitive to light elements, such as oxygen (O), due to their low atomic numbers and weak characteristic X-ray emission. As a result, oxygen is not detected by XRF, even though it is present in the $BiFeO_3$ crystal structure. The absence of other detectable elements also suggests a lack of heavy-element impurities, supporting the sample's phase purity which was previously validated by XRD analysis. With a near-ideal stoichiometry, the identical between the measured and calculated values verify the accomplished synthesis of $BiFeO_3$.

The UV-Visible Spectroscopy characterization provides the diffuse reflectance spectrum (DRS) of as-synthesized $BiFeO_3$ powder counter to incident wavelength of light, considered within the UV-Visible range. In the 525–580 nm range, the spectrum highlights a notable reduction in reflectance, indicating a powerful absorption band within the range of visible light (Ayala et al., 2020). This marked decline in reflectance shows electronic transitions that enfold the excitation of electrons migrating from the oxygen 2p orbitals detected within the valence band to the iron 3d orbitals situated in the conduction band. This transition can be ascribed to the CT process typically observed in $BiFeO_3$, which underscores its semiconductor characteristics and responsiveness to visible light (Ayala et al., 2020). The proportion to absorb light in this spectrum is necessary for optoelectronic and photocatalytic applications. This also assists photo-induced charge transfer in Surface-Enhanced Raman Spectroscopy (SERS).

The function transforms the reflectance data into absorbance-like values using Eq. (1):

$$[F(R)hv]^n = A\ (hv - E_g) \tag{1}$$

which $F(R)$ is the Kubelka-Munk function, hv is the photon energy, E_g is the bandgap energy, and n depends on the type of electronic transition (n = 2 for direct allowed transitions, which is applicable to $BiFeO_3$). By plotting $[F(R)hv]^n$ versus hv, and extrapolating the linear portion to the x-axis, the direct bandgap was expected to be 2.1 eV. The gained value is located within the expected parameters for $BiFeO_3$ and displays remarkable concordance with the literature values regarding the potent bandgap of $BiFeO_3$ (Ayala et al., 2020). The relatively tiny bandgap authorizes coherent absorption of visible light and eases electron excitation under low-energy irradiation. This bandgap has also been indicated to be potent in dye degradation as showed by prior investigations (Ilić et al., 2025), (Caglar et al., 2021) highlighting it's prospective to increase dye detection through SERS. The analysis of UV-Vis diffuses reflectance and bandgap substantiate that the synthesized $BiFeO_3$ shows robust absorption of visible light and possesses a fit bandgap energy. These findings reinforce $BiFeO_3$'s potential application as a semiconductor-based SERS substrate with mechanisms of improvement fueled by CT.

Three contrasting substrates were inspected: bare SiO_2, $BiFeO_3$ on SiO_2, and Rhodamine B placed on the $BiFeO_3$ ply. As showed in the figure, Rhodamine B on bare SiO_2 builds no clear Raman peaks from the dye, implying that plain silicon dioxide does not provide any Raman enhancement. This observation confirms that SiO_2 alone is not suitable for SERS applications due to its poor ability to amplify Raman signals. In contrast, the Raman spectrum of the $BiFeO_3$ substrate without Rhodamine B displays distinct intrinsic peaks that are the characteristics of $BiFeO_3$. Specifically, peaks appear

at 370 cm^{-1} and 470 cm^{-1}, which correspond to E modes, and a peak at 520 cm^{-1}, assigned to the A_1 mode, consistent with previous reports on rhombohedral $BiFeO_3$ (see Table 3). These phonon modes originate from lattice vibrations of the Bi and Fe ions in the perovskite structure and serve as reference points for the substrate's baseline Raman activity. Remarkably, when Rhodamine B is adsorbed onto the $BiFeO_3$ substrate, the resulting SERS spectrum (blue line) reveals a significant enhancement in Raman signal intensity across multiple Rhodamine B-specific vibrational modes. This enhancement confirms that the $BiFeO_3$ substrate is capable of amplifying the Raman signal of Rhodamine B through the chemical enhancement mechanism, primarily driven by photoinduced CT between the Rhodamine B molecules and the $BiFeO_3$ surface. The absence of plasmonic metals in this system supports the conclusion that the enhancement originates from the semiconductor-based SERS activity of $BiFeO_3$. Several well-known Raman peaks of Rhodamine B are clearly visible and assigned based on literature references (Table 3). For instance, peaks at 616 cm^{-1} and 933 cm^{-1} are asigned to Cx–Cx–Cx bending vibrations, while the 765 cm^{-1} peak corresponds to C–H out-of-plane bending (Mao et al., 2023). Peaks at 1079 cm^{-1}, 1193 cm^{-1}, and 1273 cm^{-1} are related to C–H stretching, C–C bridge band stretching, and C–H bending, respectively. Additionally, prominent aromatic C–C stretching vibrations are observed at 1357 cm^{-1}, 1510 cm^{-1}, and 1640 cm^{-1}, which are characteristic fingerprint regions of the xanthene ring system in Rhodamine B (Mao et al., 2023).

The appearance and enhancement of these distinct Rhodamine B peaks in the presence of $BiFeO_3$ confirm the suitability of $BiFeO_3$ as an effective SERS substrate, capable of detecting trace amounts of Rhodamine B. While the enhancement may not reach the level typically achieved with noble-metal-based substrates, the results demonstrate that $BiFeO_3$ offers a promising and sustainable alternative, particularly for applications prioritizing environmental safety and cost-effectiveness.

Conclusion

In this study, we successfully synthesized lead-free bismuth ferrite ($BiFeO_3$) perovskite via the sol–gel method and fabricated a $BiFeO_3$-based SERS substrate using a simple drop-casting approach. XRD analysis confirmed the formation of a single-phase rhombohedral perovskite structure with high crystallinity and no detectable impurity phases. Optical characterization revealed a direct bandgap of 2.1 eV, supporting strong absorption in the visible light region and confirming the material's suitability for light-responsive applications. Notably, the $BiFeO_3$ substrate demonstrated a significant enhancement of the Raman signal of Rhodamine B, enabling detection down to 10 ppm with well-resolved vibrational modes. This SERS activity is attributed to the CT mechanism enabled by the semiconducting properties of $BiFeO_3$ and its effective interaction with Rhodamine B molecules. These results represent the first demonstration of pure $BiFeO_3$ as a non-plasmonic, lead-free SERS substrate for dye detection, showcasing its potential as a cost-effective, chemically stable, and environmentally friendly alternative to noble metals. These findings open new directions for the design of sustainable SERS platforms for environmental monitoring, food safety, and chemical sensing applications.

Acknowledgment

We are deeply grateful to the University of Indonesia (UI) for supporting this research through grant No. PKS-591/UN2.RST/HKP.05.00/2025. We also thank the National Research and Innovation Agency (BRIN) for additional funding under the RP 2025 ORNM Grant. The authors sincerely appreciate the Advanced Characterization Laboratory (ELSA-BRIN) at BRIN KST BJ Habibie, Tangerang Selatan, Indonesia, for access to facilities and valuable technical assistance. D.C.M. acknowledges support from the Degree by Research (DbR) program of BRIN.

Compliance with ethics guidelines

The authors declare they have no conflict of interest or financial conflicts to disclose.

This article contains no studies with human or animal subjects performed by authors.

DOI: 10.5614/j.eng.technol.sci.2025.57.6.10

References

Abdillah, M. N., & Triyono, D. (2019). Structural properties of bismuth ferrite synthesized by sol-gel method with variation of calcination temperature. *Journal of Physics: Conference Series*, *1245*, 012087.

Anucha, C. B., Guenin, E., & Percot, A. (2025). Embedded nanoparticle silk fibroin hydrogel as surface enhanced Raman scattering (SERS) substrates for detection of methylene blue in water. *Materials Today Sustainability*, *31*, 101169.

Ayala, Z. B., Peñalva, J. J., Hernández, J. M., Loro, H., & Eyzaguirre, C. R. (2020). Study of the optical and photovoltaic properties in nanoparticles of $BiFeO_3$. *Journal of Physics: Conference Series*, *1558*, 012010.

Bashir, N., Ali, T., Khan, I., Habib, A., Iqbal, N., & Afzal, A. (2025). Ultrasensitive carbon nitride nanosheets for multiplex sensing of rhodamine B and methylene blue. *Diamond and Related Materials*, *153*, 112073.

Cheng, X.-L., Fu, T.-R., Zhang, D.-F., Xiong, J.-H., Yang, W.-Y., & Du, J. (2023). Biomass-assisted fabrication of rGO-AuNPs as surface-enhanced Raman scattering substrates for in-situ monitoring methylene blue degradation. *Analytical Biochemistry*, *667*, 115087.

Culbertson, C. M., Flak, A. T., Yatskin, M., Cheong, P. H.-Y., Cann, D. P., & Dolgos, M. R. (2020). Neutron total scattering studies of group II titanates ($ATiO_3$, A^{2+} = Mg, Ca, Sr, Ba). *Scientific Reports*, *10*, 3729.

Caglar, B., Guner, E. K., Özdokur, K. V., Özdemir, A. O., İçer, F., Caglar, S., Doğan, B., Beşer, B. M., Çırak, Ç., Tabak, A., & Ersoy, S. (2021). Application of BiFeO3 and Au/BiFeO3 decorated kaolinite nanocomposites as efficient photocatalyst for degradation of dye and electrocatalyst for oxygen reduction reaction. *Journal of Photochemistry and Photobiology A: Chemistry*, *418*, 113400.

Cui, S., Tian, C., Zhu, J., Wang, L., Han, D., & Peng, L. (2025). MoS2@Ag composite structure for surface-enhanced Raman scattering. *Journal of Alloys and Compounds*, *1029*, 180800.

Fajriyani, F. & Triyono, D. Effect of Zr doped Bi site in bismuth ferrite on crystal structure and optical bandgap (2020). *AIP Conference Proceedings*, 2242.

Hidayah, A. N., Triyono, D., Herbani, Y., & Saleh, R. (2022). Liquid surface-enhanced raman spectroscopy (Sers) sensor-based au-ag colloidal nanoparticles for easy and rapid detection of deltamethrin pesticide in brewed tea. *Crystals*, *12*(1).

Hidayah, A. N., Triyono, D., Herbani, Y., & Saleh, R. (2021). Effect of silver nanoparticle yield in enhancing Raman signal of SERS substrate fabricated on Whatman filter paper. *Journals of Physics and Its Applications*, *4*(2), 47-50.

Ilić, N. I., Radojković, A., Vijatović Petrović, M. M., Bobić, J., Džunuzović, A., Rajić, V., & Stojanović, B. (2025). The role of leached iron from BiFeO3 photocatalyst for water treatment. *Colloids and Surfaces A: Physicochemical and Engineering Aspects*, *720*, 137131.

Jain, A., Wang, Y. G., Kumar, A., Gupta, N., Kumar, K., & Goyal, A. K. (2025). BiFeO3-based lead-free materials: Recent breakthroughs and their multifunctional applications. *Journal of Alloys and Compounds*,*1010*, 177170.

Kokilavani, V., Kannan, S., & Manikandan, S. (2022). Recent advances in degradation of organic pollutants in aqueous solutions using bismuth-based photocatalysts: A review. *Chemosphere*, *304*, 135321.

Liu, G., Karuturi, S. K., Chen, H., Wang, D., Ager, J. W., Simonov, A. N., & Tricoli, A. (2020). Enhancement of the photoelectrochemical water splitting by perovskite $BiFeO_3$ via interfacial engineering. *Solar Energy*, *202*, 198–203.

Mao, S., Pei, F., Feng, S., Hao, Q., Zhang, P., Tong, Z., Mu, X., Lei, W., & Liu, B. (2023). Detection of trace Rhodamine B using stable, uniformity, and reusable SERS substrate based on Ag@SiO2-Au nanoparticles. *Colloids and Surfaces A: Physicochemical and Engineering Aspects*, *657*, 130595.

Cebela, M., Zagorac, D., Batalovic, K., Radakovic, J., Stojadinovic, B., Spasojevic, V., Hercigonja, R. (2017). $BiFeO_3$ perovskite : A multidisciplinary approach to multiferroics. *Ceramics International*, *43*,1256-1264.

Mhamad, S. A., Ali, A. A., Mohtar, S. S., Aziz, F., Aziz, M., Jaafar, J., Yusof, N., Wan Salleh, W. N., Ismail, A. F., & Chandren, S. (2022). Synthesis of bismuth ferrite by sol-gel auto combustion method: Impact of citric acid concentration on its physicochemical properties. *Materials Chemistry and Physics*, *282*, 125983.

Nithish, G., Prashanth, S., Chandru, S., & Moushmi, A. (2025). A review article on the sweet scandal: The truth behind rhodamine B. *Global Journal of Health Sciences and Research*, *3*, 18-20.

Pan, N., Shi, Z., Wu, P., Xi, H., Gao, Y., You, T., & Yin, P. (2022). Surface enhanced Raman scattering of adsorbates on Au-CsPbIBr2 perovskite-based nanocomposites: charge-transfer and electromagnetic enhancement. *Nanoscale*, *14*(29), 10469–10476.

Pan, N., Tian, J., Shi, Z., Zhang, W., Gao, Y., You, T., & Yin, P. (2023). Investigation of sensitive SERS detection via a perovskite-coated Ag nanofilm. *Journal of Materials Chemistry* C, *11*, 13256-13262.

Sahoo, P., Tiwari, C., Kukreti, S., & Dixit, A. (2024). All oxide lead-free bismuth ferrite perovskite absorber based FTO/ZnO/BiFeO3/Au solar cell with efficiency ∼ 12%: First principle material and macroscopic device simulation studies. *Journal of Alloys and Compounds*, *981*, 173599.

Sarkar, K., Harsh, H., Rahman, Z., & Kumar, V. (2024). Enhancing the structural, optical, magnetic and ferroelectric properties of perovskite BiFeO3 through metal substitution. *Chemical Physics Impact, 8*, 100478.

Triyono, D., Laysandra, H., & Liu, H. L. (2019). Structural, optical, and dielectric studies of $LaFe_{1-x}Mo_xO_3$ (x = 0.0, 0.5) perovskite materials. Journal of Materials Science: *Materials in Electronics*, *30*, 2512-2522.

Wang, J., Qiu, C., Pang, H., Wu, J., Sun, M., & Liu, D. (2021). High-performance SERS substrate based on perovskite quantum dot-graphene/nano-Au composites for ultrasensitive detection of rhodamine 6G andp-nitrophenol. *Journal of Materials Chemistry C*, *9*(28), 9011–9020.

Wang, Q., Wu, Y., Wang, Y., Mei, R., Zhao, R., Wang, X., & Chen, L. (2025). Surface enhanced Raman scattering tag enabled ultrasensitive molecular identification of Hippocampus trimaculatus based on DNA barcoding. *Talanta*, *294*, 128289.

Yin, Z., Li, Y., Xu, J., Qian, Z. F., & Xiong, K. (2022). Recent advances of perovskite materials for surface enhanced Raman scattering and their applications. *Materials Today Physics* , *27,* 100815.

Zhou, T., Zhai, T., Shen, H., Wang, J., Min, R., Ma, K., & Zhang, G. (2023). Strategies for enhancing performance of perovskite bismuth ferrite photocatalysts (BiFeO3): A comprehensive review. *Chemosphere*, *339*, 139678.

Zhuang, Z., Wang, J., Huang, J., Hong, R., Tao, C., Wang, Q., Lin, H., Han, Z., Zhang, D., & Zhuang, S. (2024). Fabrication of High-Stability and -Sensitivity Perovskite Nanoparticles with a Core–Shell Structure for Surface-Enhanced Raman Scattering. *The Journal of Physical Chemistry C*, *128*(24), 10120–10132

Manuscript Received: 24 April 2025
Revised Manuscript Received: 7 July 2025
Accepted Manuscript: 15 September 2025